Am J Transl Res 2026;18(8):7405-7419
www.ajtr.org /ISSN:1943-8141/AJTR0174095

Original Article

Norcantharidin induces apoptosis in hepatocellular carcinoma MHCC97-H cells in association with altered NF-κB/IκBα signaling dynamics and JNK activation

Dong Wang*, Jinbo Guo*, Xiaolan Zhang, Fengrong Yin, Donglai Cui

*Department of Gastroenterology, The Second Hospital of Hebei Medical University, Shijiazhuang 050035, Hebei, China. *Equal contributors.*

Received May 16, 2026; Accepted July 12, 2026; Epub August 15, 2026; Published August 30, 2026

Abstract: Norcantharidin (NCTD), a demethylated derivative of cantharidin, has antitumor activity against multiple cancer types; however, its effects on the NF-κB/JNK signaling axis in hepatocellular carcinoma (HCC) remain incompletely defined. MHCC97-H HCC cells were treated with NCTD at 5, 20, and 40 μg/mL (approximately 29.7, 118.9, and 237.9 μM), alone or in combination with pyrrolidine dithiocarbamate (PDTC, 50 μM), a compound with reported NF-κB inhibitory and antioxidant properties. NCTD suppressed cell viability in a dose- and time-dependent manner, with 48-h inhibition rates of 24.3%, 51.9%, and 72.1% at the three concentrations. Based on the available MTS data, the estimated NCTD IC50 was > 40 μg/mL at 24 h and approximately 19.0 μg/mL at 48 h. Flow cytometry showed corresponding apoptosis rates of 13.3%, 36.8%, and 43.2%, which increased to 50.2% after PDTC co-treatment. Western blotting showed reduced nuclear NF-κB p65 signal and decreased cytoplasmic IκBα levels, together with increased phosphorylated JNK (p-JNK), while total JNK remained unchanged. RT-qPCR showed upregulation of pro-apoptotic Bax, downregulation of anti-apoptotic Bcl-2, and increased c-Jun, TNF-α, and IL-6 transcripts. NCTD further impaired colony formation, induced G0/G1 arrest, depolarized mitochondrial membrane potential, and increased reactive oxygen species. TCGA-LIHC bulk RNA-seq data were analyzed to provide clinical context. NF-κB pathway genes were differentially expressed in HCC, and enrichment analyses implicated NF-κB, apoptosis, TNF, and MAPK-related pathways. The NF-κB Core activity score showed no significant tumor-normal difference, but immune infiltration analysis revealed associations between NF-κB activity and the HCC immune microenvironment. These findings indicate that NCTD triggers mitochondrial apoptosis in MHCC97-H cells in association with reduced nuclear p65 signal, altered IκBα turnover, stress/inflammatory gene induction, and enhanced JNK activation, rather than demonstrating uniform blockade of the entire NF-κB pathway.

Keywords: Norcantharidin, NF-κB, JNK, apoptosis, hepatocellular carcinoma, TCGA

Introduction

Hepatocellular carcinoma (HCC) is among the most common digestive malignancies and has a poor prognosis because it often develops insidiously and progresses rapidly [1]. In China, where the disease burden is high, there remains a need to identify effective therapeutic agents and clarify their mechanisms of action [2].

Norcantharidin (NCTD), a demethylated derivative of cantharidin, retains anticancer activity while markedly reducing the bone marrow, gastrointestinal, and urinary tract toxicities that limit clinical use of cantharidin [3]. NCTD has been reported to inhibit proliferation and induce cell death in hepatocellular carcinoma, breast cancer, cervical cancer, colorectal cancer, and other malignancies [4, 5], and it has been used clinically in hepatic and esophageal cancers. Beyond its antitumor activity, NCTD has also been associated with increased peripheral leukocyte counts and immunomodulatory effects [6].

The transcription factor NF-κB occupies a central and context-dependent position in the molecular context of HCC [7]. Aberrant activation of NF-κB in liver tumors drives expression of genes involved in cell survival, proliferation, and inflammatory responses [8]. Under basal conditions, NF-κB is retained in the cytoplasm

https://doi.org/10.62347/CLVD1603

by inhibitory IκB proteins, predominantly IκBα. Upon stimulation by cytokines, viral proteins, or genotoxic stress, IκBα undergoes phosphorylation and proteasomal degradation, allowing NF-κB nuclear translocation and target gene activation [9]. In the chronically inflamed liver, the background against which most HCC arises, sustained NF-κB activation creates a microenvironment permissive to malignant transformation [10].

Because NF-κB signaling is regulated at multiple levels, including IκBα turnover, p65 nuclear localization, post-translational modification, and inflammatory transcriptional feedback, transcriptomic activity scores from bulk tumor tissue should be interpreted as contextual evidence rather than as a direct surrogate for nuclear p65 activity in cultured cells.

The c-Jun N-terminal kinase (JNK) pathway regulates apoptosis, differentiation, and inflammation and represents a stress-responsive branch of the MAPK signaling network [11]. NF-κB and JNK also interact functionally: in inflammatory contexts, activated NF-κB can limit excessive JNK activation and support cell survival, whereas NF-κB blockade can permit sustained JNK activation and promote cell death [12]. This interaction suggests that pharmacologic attenuation of NF-κB activity may suppress tumor cell survival not only through transcriptional reprogramming but also through reactivation of pro-apoptotic JNK signaling.

Although NCTD has a documented anticancer profile, its effects on the NF-κB/JNK signaling interface in hepatocellular carcinoma remain incompletely defined. In this study, MHCC97-H cells were treated with increasing concentrations of NCTD, either alone or in combination with pyrrolidine dithiocarbamate (PDTC), a pharmacologic modulator with reported NF-κB inhibitory and antioxidant activities. We evaluated proliferation, apoptosis, NF-κB/JNK-associated protein changes, apoptosis-related gene transcription, mitochondrial membrane potential, and reactive oxygen species production. To place the in vitro findings in a broader clinical context, TCGA-LIHC bulk RNA-seq data were analyzed for NF-κB pathway gene expression, enrichment patterns, and immune microenvironment associations.

Materials and methods

Cell culture and reagents

The authenticated MHCC97-H human hepatocellular carcinoma cell line was obtained from the Cell Bank of the Chinese Academy of Sciences, Shanghai Institute of Biochemistry and Cell Biology (catalog/serial no. 19375.09.3101HUMSCSP5092; CAS, China). Cells were authenticated by short tandem repeat profiling before use, and mycoplasma contamination was routinely excluded using the MycoAlert Detection Kit (Lonza, LT07-318). Cells were maintained at 37°C in a humidified 5% CO_2 incubator in Dulbecco's modified Eagle's medium (DMEM; Gibco, 11995065) supplemented with 10% fetal bovine serum (Thermo Fisher, 16000044), 100 U/mL penicillin, and 100 μg/mL streptomycin (Thermo Fisher, 15140122).

Norcantharidin (NCTD; N2638; purity ≥ 98%) was obtained from Sigma-Aldrich and dissolved in DMSO to prepare stock solutions. Working concentrations of 5, 20, and 40 μg/mL, corresponding approximately to 29.7, 118.9, and 237.9 μM based on the molecular weight of NCTD (168.15 g/mol), were freshly prepared in culture medium before each experiment. Pyrrolidine dithiocarbamate (PDTC; Sigma-Aldrich, P8765), a compound reported to modulate NF-κB signaling and oxidative-stress responses, was used at a final concentration of 50 μM. Treatment duration ranged from 12 to 48 h depending on the assay.

Cell proliferation assay

Cell viability was measured using the CellTiter 96 AQueous One Solution MTS assay (Promega, G3582). MHCC97-H cells were plated at 5×10^3 cells/well in 96-well plates and allowed to adhere overnight. After 12, 24, 36, or 48 h of treatment with NCTD, PDTC, or both, MTS reagent (20 μL/well) was added, and cells were incubated for an additional 2-4 h at 37°C. Absorbance was measured at 490 nm using a BioTek Synergy HTX microplate reader. Proliferation inhibition rates were calculated relative to untreated controls. Because the available concentration-response series included three NCTD concentrations, IC50 values were

estimated descriptively from the MTS inhibition data; if 50% inhibition was not reached at the highest tested concentration, the IC50 was reported as greater than 40 μg/mL (> 237.9 μM).

Hoechst 33342 nuclear staining

Apoptotic nuclear morphology was assessed using the Hoechst 33342 Staining Kit (Thermo Fisher, H3570). Cells cultured on glass coverslips were treated as indicated, stained with Hoechst 33342 (5 μg/mL, 15 min, 37°C), and observed with a Zeiss Axio Observer fluorescence microscope. Nuclear condensation and fragmentation were identified as characteristic apoptotic features.

Annexin V-FITC/PI flow cytometry

Apoptosis was measured using an apoptosis detection kit (Thermo Fisher, V13242). Cells were harvested, washed with PBS, and stained with Annexin V-FITC and propidium iodide (PI) according to the manufacturer's instructions. Data were collected using a BD FACSCanto II flow cytometer and analyzed with FlowJo v10 to distinguish viable, early apoptotic, late apoptotic, and necrotic populations.

Caspase-3/7 activity assay

Caspase-3/7 enzymatic activity was measured using the Caspase-Glo 3/7 Assay Kit (Promega, G8091). Cells were seeded in white 96-well plates, treated as indicated, and incubated with Caspase-Glo reagent for 1 h at room temperature. Luminescence was measured using a BioTek Synergy HTX reader and normalized to untreated controls.

Mitochondrial membrane potential (ΔΨm) assay

The JC-1 probe (Thermo Fisher, T3168) was used to assess mitochondrial membrane potential. Treated cells were incubated with 2 μM JC-1 for 30 min at 37°C, washed twice with PBS, and imaged with a Zeiss Axio Observer microscope using filters appropriate for JC-1 aggregates (red) and monomers (green). The red/green fluorescence intensity ratio was calculated with ImageJ as an indicator of mitochondrial depolarization.

Intracellular ROS detection

Intracellular ROS levels were measured using CM-H_2DCFDA (Thermo Fisher, C6827). After treatment, cells were incubated with 10 μM CM-H_2DCFDA for 30 min at 37°C in the dark, washed with PBS, and visualized by fluorescence microscopy. Relative fluorescence intensity was quantified with ImageJ.

Western blotting

Total, nuclear, and cytoplasmic protein fractions were prepared from treated cells using RIPA buffer (Thermo Fisher, 89901) supplemented with protease and phosphatase inhibitors (Thermo Fisher, 78442). Nuclear-cytoplasmic fractionation was performed with the NE-PER Kit (Thermo Fisher, 78833). Protein concentrations were determined by BCA assay (Thermo Fisher, 23225). Equal amounts of protein (30 μg) were separated by SDS-PAGE and transferred to PVDF membranes (Thermo Fisher, 88518). Membranes were blocked with 5% non-fat milk and incubated overnight at 4°C with primary antibodies against NF-κB p65 (CST, 8242, 1:1000), IκBα (CST, 4814, 1:1,000), p-JNK (CST, 9251, 1:1,000), total JNK (CST, 9252, 1:1,000), β-actin (Sigma, A5441, 1:5000), Lamin B1 (Abcam, ab16048, 1:1,000), and GAPDH (Sigma, G9545, 1:5,000). After incubation with HRP-conjugated secondary antibodies (Thermo Fisher, 31460, 1:5,000), protein bands were visualized with ECL substrate (Thermo Fisher, 32106) and quantified using ImageJ.

RNA extraction and RT-qPCR

Total RNA was extracted from MHCC97-H cells using the RNeasy Mini Kit (Qiagen, 74104). Complementary DNA was synthesized from 1 μg of total RNA using the High-Capacity cDNA Reverse Transcription Kit (Thermo Fisher, 4368813). Commercial TaqMan Gene Expression Assays (Thermo Fisher), rather than custom SYBR Green primer pairs, were used for Bax (Hs00180269_m1), Bcl-2 (Hs00608023_m1), c-Jun (Hs01103582_s1), TNF-α (Hs01113624_g1), and IL-6 (Hs00985639_m1), with GAPDH (Hs02758991_g1) as the endogenous control. Quantitative PCR was performed on a QuantStudio 6 Flex system, and relative expression was calculated using the 2-ΔΔCt method.

Colony formation assay

MHCC97-H cells (500 cells/well) were seeded in 6-well plates and treated with NCTD, PDTC, or both. Cells were cultured for 10-14 days with medium replacement every 2-3 days, fixed with 4% paraformaldehyde, and stained with 0.1% crystal violet (Thermo Fisher, C3886). Colonies containing more than 50 cells were counted manually under a light microscope.

Cell cycle analysis

After treatment, cells were harvested, fixed in 70% ethanol at -20°C overnight, and stained with PI/RNase Staining Solution (Thermo Fisher, 00-6990-50) for 30 min at 37°C. DNA content was measured on a BD FACSCanto II flow cytometer, and cell-cycle distribution was analyzed with FlowJo v10.

IF staining

Cells were fixed, permeabilized, and blocked with 5% BSA. Cells were incubated overnight at 4°C with primary antibodies against NF-κB p65 (CST, 8242) and p-JNK (CST, 9251), followed by Alexa Fluor-conjugated secondary antibodies (Thermo Fisher). Nuclei were counterstained with Hoechst 33342. Images were acquired on a Zeiss Axio Observer fluorescence microscope.

TCGA bioinformatics analysis

Transcriptomic RNA-seq data (unstranded counts) for the TCGA-LIHC cohort were retrieved using the TCGAbiolinks R package, comprising 374 HCC tumor specimens and 50 adjacent normal tissues [13]. Data preprocessing included TPM normalization, log2(TPM+1) transformation, removal of duplicate gene symbols by retaining the highest-expressed record, and filtering of low-expression genes (row means > 1). For the tumor-normal NF-κB activity score comparison, 371 primary tumor samples and 50 normal samples with complete annotations were used.

Differential expression analysis between tumor and normal groups was performed with the limma package using a design matrix contrasting Tumor versus Normal, with Benjamini-Hochberg multiple-testing correction [14]. Differentially expressed genes (DEGs) were defined by $|\log2FC| > 1$ and adjusted $P < 0.05$. NF-κB pathway-related genes, including RELA, NFKBIA, NFKB1, IKBKB, CHUK, RELB, NFKB2 (core NF-κB), BAX, BCL2, BCL2L1 (apoptosis), TNF, IL6, IL1B (inflammation), and JUN, MAPK8, MAPK9 (JNK cascade), were annotated on volcano plots when significantly differentially expressed.

GO and KEGG enrichment analyses were conducted with the clusterProfiler package using Benjamini-Hochberg correction [15]. Immune cell infiltration was evaluated by single-sample gene set enrichment analysis (ssGSEA) across 22 immune cell types using the GSVA package [16]. NF-κB pathway activity scores were computed by ssGSEA/GSVA using the core genes RELA, NFKBIA, NFKB1, IKBKB, CHUK, RELB, and NFKB2. Tumor-normal score distributions were compared using the Wilcoxon rank-sum test, and Spearman correlation was calculated between NF-κB activity and immune cell infiltration scores.

Statistical analysis

All in vitro laboratory experiments were performed independently three times, and results are presented as mean ± SD. Statistical analyses were performed using GraphPad Prism version 9. One-way analysis of variance (ANOVA) followed by Tukey's post hoc test was used for laboratory experiments. Pearson correlation was used for the experimental correlations between nuclear p65 or p-JNK levels and apoptosis rate. For bioinformatic analyses, group comparisons were performed using the Wilcoxon rank-sum test, and correlations between NF-κB activity scores and immune infiltration scores were assessed using Spearman's rank correlation coefficient. $P < 0.05$ was considered statistically significant.

Results

NCTD inhibits MHCC97-H cell proliferation

Exposure of MHCC97-H cells to NCTD produced a dose- and time-dependent reduction in cell viability. At 5 μg/mL (29.7 μM), inhibition remained below 25% across all time points. Higher concentrations of 20 and 40 μg/mL (118.9 and 237.9 μM, respectively) progressively suppressed proliferation over the 48-h observation period, with curves diverging from

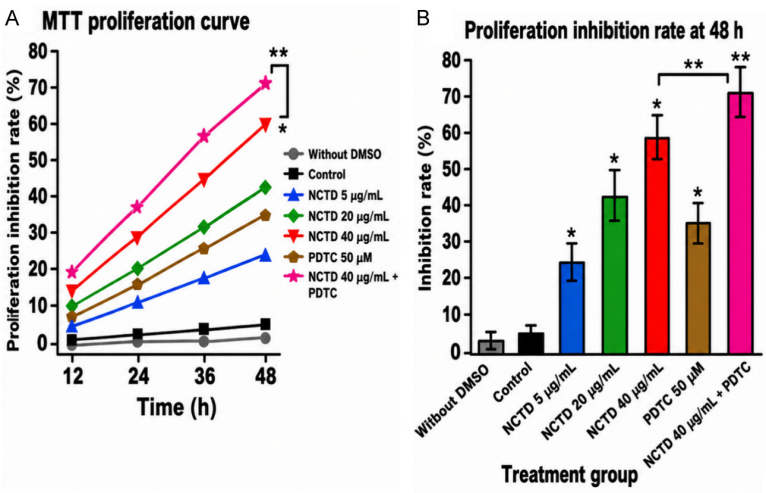

Figure 1. NCTD inhibits MHCC97-H cell proliferation. A. MTS proliferation curves of cells treated with NCTD (5, 20, and 40 μg/mL; approximately 29.7, 118.9, and 237.9 μM), PDTC (50 μM), or NCTD 40 μg/mL + PDTC over 12-48 h. B. Proliferation inhibition rates at 48 h. Based on the available MTS data, the estimated NCTD IC50 was > 40 μg/mL (> 237.9 μM) at 24 h and approximately 19.0 μg/mL (approximately 113.0 μM) at 48 h. Data are mean ± SD, n = 3. *P < 0.05, **P < 0.01 vs. control; ##P < 0.01 vs. NCTD 40 μg/mL.

the control as early as 12 h (**Figure 1A**). At 24 h, the 50% inhibition threshold was not reached even at 40 μg/mL, so the estimated 24-h IC50 was > 40 μg/mL (> 237.9 μM). At 48 h, proliferation inhibition rates were 24.3 ± 2.1%, 51.9 ± 3.0%, and 72.1 ± 4.2% in the 5, 20, and 40 μg/mL groups, respectively (**Figure 1B**), giving an interpolated 48-h IC50 of approximately 19.0 μg/mL (approximately 113.0 μM). PDTC alone (50 μM) inhibited proliferation by 39.8 ± 2.5%, whereas NCTD 40 μg/mL combined with PDTC produced the strongest inhibition (85.3 ± 3.6%; P < 0.01 vs. NCTD 40 μg/mL alone).

NCTD induces apoptosis in MHCC97-H cells

Hoechst 33342 staining of cells treated with 40 μg/mL NCTD revealed time-dependent increases in apoptotic nuclear features, including chromatin condensation and nuclear fragmentation. Quantification of apoptotic nuclei yielded rates of 11.2 ± 0.2%, 19.8 ± 0.8%, 28.0 ± 1.0%, and 34.1 ± 1.0% at 12, 24, 36, and 48 h, respectively (P < 0.05 for each time point vs. control; **Figure 2A**, **2B**).

Annexin V-FITC/PI flow cytometry showed that after 48 h of treatment, total apoptosis rates (early + late apoptosis) were 13.3 ± 1.2%, 36.8 ± 2.7%, and 43.2 ± 3.1% for 5, 20, and 40 μg/mL NCTD, respectively (**Figure 2C**, **2D**). PDTC alone induced 17.5 ± 1.4% apoptosis, while NCTD 40 μg/mL combined with PDTC increased the total apoptotic fraction to 50.2 ± 2.9% (P < 0.01 vs. NCTD alone).

NCTD modulates NF-κB and JNK signaling

Nuclear and cytoplasmic protein fractions were analyzed by Western blotting. NCTD dose-dependently reduced nuclear NF-κB p65 signal, with quantified decreases to 0.80 ± 0.05-fold, 0.67 ± 0.04-fold, and 0.45 ± 0.03-fold at 5, 20, and 40 μg/mL, respectively (P < 0.01; **Figure 3A**, **3B**). Cytoplasmic IκBα levels also decreased (0.78 ± 0.04-fold, 0.63 ± 0.03-fold, and 0.42 ± 0.03-fold; P < 0.01; **Figure 3A**, **3C**), indicating altered IκBα turnover rather than simple evidence of uniform NF-κB pathway inhibition. NCTD 40 μg/mL combined with PDTC further reduced nuclear p65 to 0.32 ± 0.02-fold and IκBα to 0.30 ± 0.02-fold (P < 0.001 vs. control).

Total JNK protein remained unchanged across all treatment conditions (P > 0.05; **Figure 3A**, **3D**), whereas p-JNK increased in a dose-dependent manner, reaching 2.7 ± 0.2-fold at 40 μg/mL NCTD and 3.6 ± 0.3-fold in the combination group (P < 0.001; **Figure 3A**, **3E**) [17].

NCTD alters apoptosis-related and inflammatory gene transcription

RT-qPCR was performed to measure five target genes: Bax, Bcl-2, c-Jun, TNF-α, and IL-6.

Pro-apoptotic Bax mRNA increased in a concentration-dependent manner, reaching 1.6 ± 0.1-, 2.2 ± 0.2-, and 3.0 ± 0.3-fold at 5, 20, and 40 μg/mL NCTD, respectively, whereas anti-apoptotic Bcl-2 was reciprocally suppressed to 0.8 ± 0.05-, 0.6 ± 0.04-, and 0.5 ± 0.03-fold (P < 0.01; **Figure 4A**, **4B**). The Bax/Bcl-2 ratio increased from approximately 1.0 in control cells to approximately 6.0 at the highest NCTD concentration, consistent with a shift toward

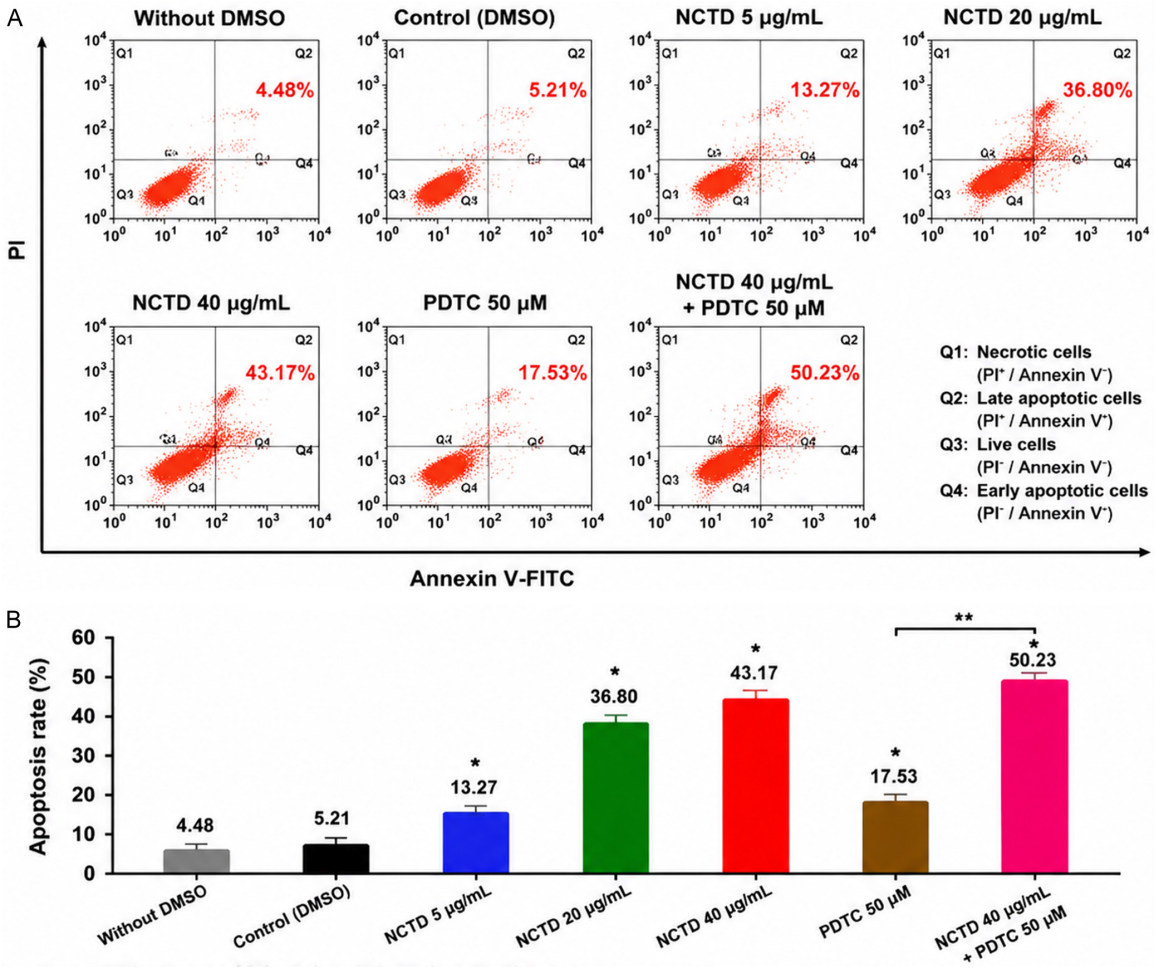

Figure 2. NCTD induces apoptosis in MHCC97-H cells. A. Representative Annexin V-FITC/PI flow cytometry dot plots of MHCC97-H cells treated with NCTD at 5, 20, or 40 μg/mL, PDTC at 50 μM, or their combination for 48 h. B. Quantification of total apoptosis rates, including early and late apoptosis. Data are presented as mean ± SD, n = 3. *P < 0.05, P < 0.01 versus the control group; ##P < 0.01 versus the NCTD 40 μg/mL group.

mitochondrial apoptotic priming. c-Jun was induced across all treatment groups (**Figure 4C**). The stress- and inflammation-related transcripts of TNF-α and IL-6 were also upregulated by NCTD (**Figure 4D**, **4E**), indicating that NCTD did not produce uniform transcriptional silencing of all NF-κB-responsive inflammatory genes. Under combination treatment, all five genes showed the greatest deviation from control levels (**Figure 4F**).

Reduced nuclear p65 signal is associated with enhanced JNK activation and apoptosis

Immunofluorescence staining visualized p65 and p-JNK at single-cell resolution. In untreated cells, nuclear p65 fluorescence was diffusely distributed with moderate intensity, whereas p-JNK signal was uniformly low (**Figure 5A**). With increasing NCTD concentration, nuclear p65 intensity progressively decreased; in cells receiving both NCTD 40 μg/mL and PDTC, p65 nuclear signal was barely detectable (**Figure 5B**). p-JNK fluorescence showed the opposite pattern, with minimal signal in control cells, moderate elevation after NCTD alone, and strong intensification under combination treatment (**Figure 5C**, **5D**). The corresponding time-course Western blot and densitometric results are presented in **Figure 5E** and **5F**.

Caspase-3/7 activity increased to 2.55 ± 0.15-fold after NCTD 40 μg/mL alone and to 3.10 ± 0.20-fold after PDTC co-treatment (P < 0.01; **Figure 5G**). Pearson correlation analysis across all seven treatment groups showed a ne-

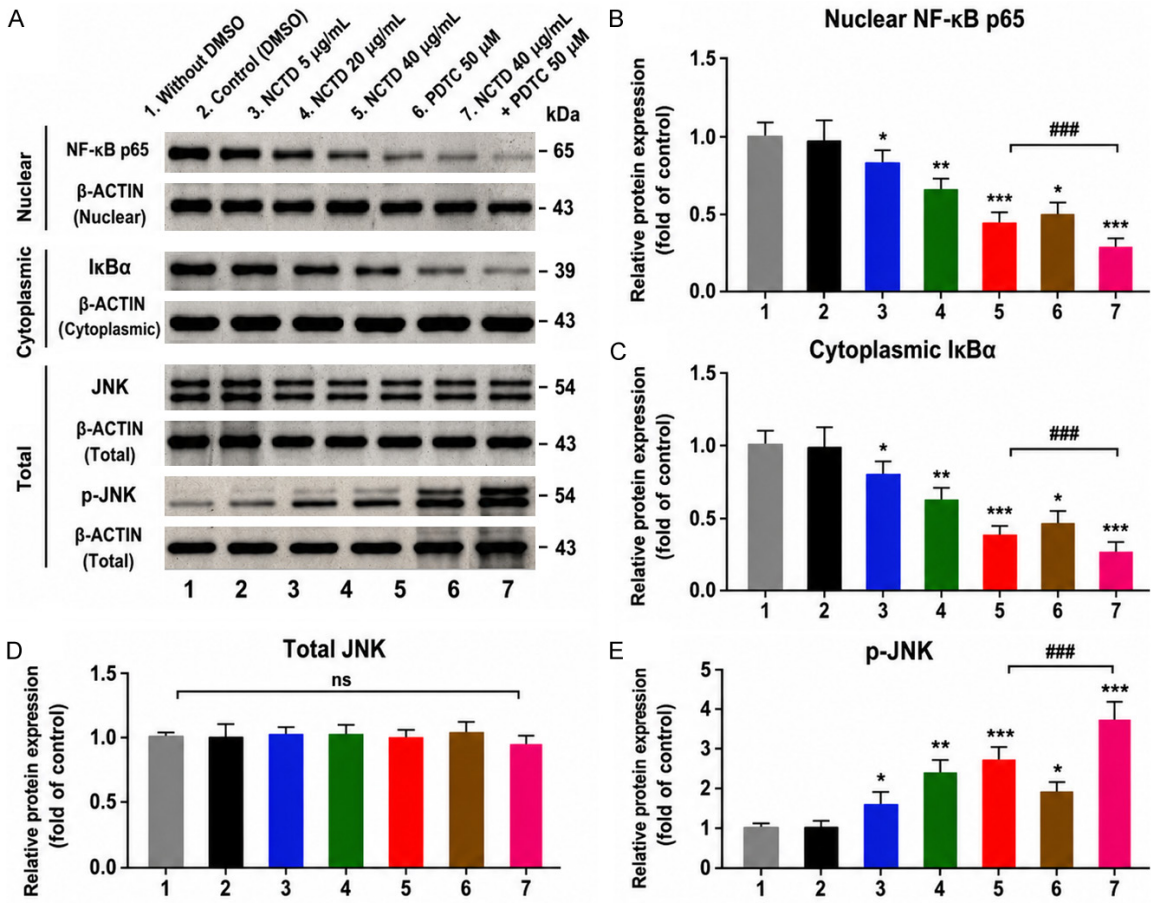

Figure 3. NCTD modulates NF-κB/IκBα and JNK signaling. A. Representative Western blots of nuclear NF-κB p65, cytoplasmic IκBα, total JNK, and p-JNK. β-actin, Lamin B1, and GAPDH served as fraction-specific loading controls. B-E. Densitometric quantification of nuclear p65, IκBα, total JNK, and p-JNK. NCTD reduced nuclear p65 signal, decreased cytoplasmic IκBα, and increased p-JNK in a dose-dependent manner; these effects were potentiated by PDTC. Data are mean ± SD, n = 3. *P < 0.05, **P < 0.01, ***P < 0.001 vs. control; ###P < 0.001 vs. NCTD 40 μg/mL; ns, not significant.

gative association between nuclear p65 levels and apoptosis (r = -0.94, P < 0.001; **Figure 5H**) and a strong positive association between p-JNK levels and apoptosis (r = 0.96, P < 0.001; **Figure 5I**).

NCTD impairs long-term proliferative capacity, induces cell cycle arrest, and triggers mitochondrial dysfunction

The colony formation assay showed a dose-dependent impairment of clonogenic survival. Colony counts were reduced to 18 ± 2% of control under combination treatment (P < 0.001; **Figure 6A**, **6B**).

Cell-cycle analysis by flow cytometry showed G0/G1 phase accumulation in NCTD-treated cells, with the G0/G1 fraction most strongly elevated in the combination group (**Figure 6C**, **6D**). The sub-G1 population also increased substantially under combination treatment.

JC-1 staining showed a treatment-related decrease in the red/green fluorescence ratio, indicating mitochondrial membrane depolarization, with the strongest effect observed in the combination group (**Figure 6E**, **6F**).

Intracellular ROS levels, measured by CM-H_2DCFDA oxidation, increased in a dose-dependent manner after NCTD treatment and peaked under combination treatment (P < 0.01; **Figure 6G**, **6H**). A schematic of the proposed signaling pathway is shown in **Figure 6I**.

TCGA analysis provides clinical context for NF-κB pathway dysregulation in HCC

RNA-seq data from the TCGA-LIHC cohort (374 HCC tumors and 50 normal liver tissues) were

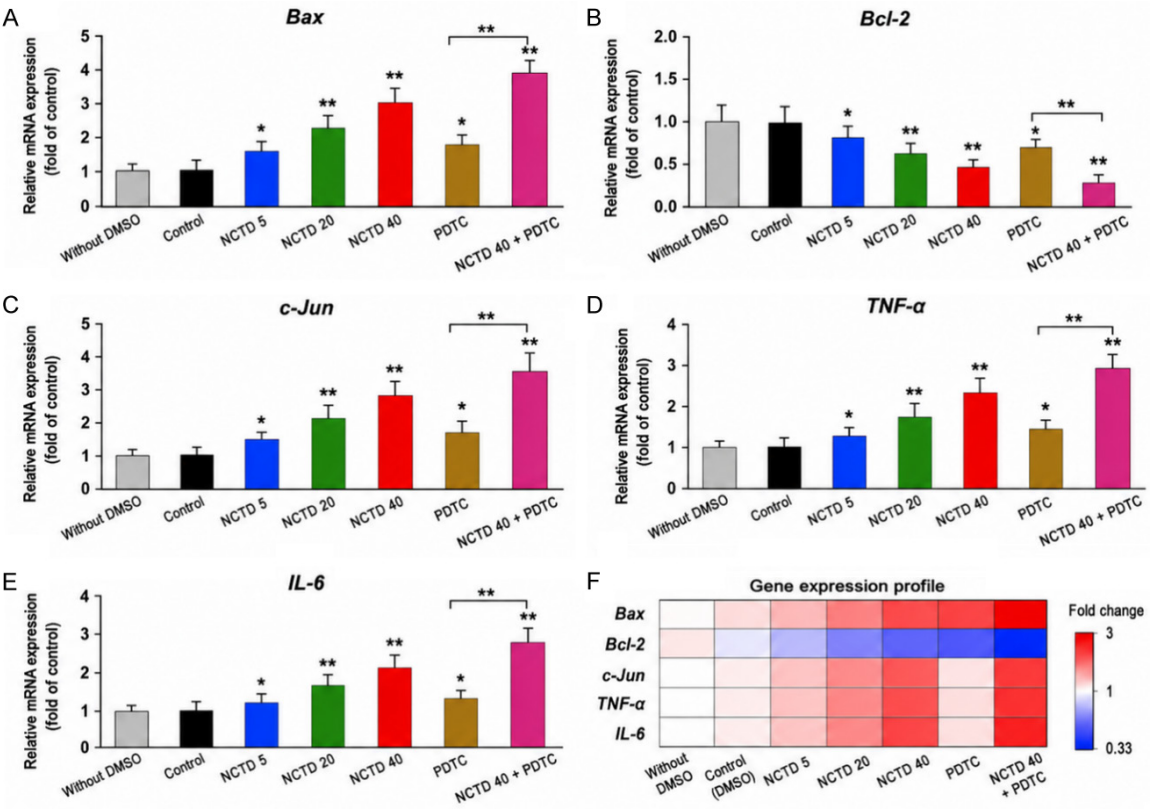

Figure 4. NCTD alters apoptosis- and stress-related gene transcription. A-E. RT-qPCR analysis of Bax, Bcl-2, c-Jun, TNF-α, and IL-6 mRNA. F. Heatmap of fold changes across all genes and treatment conditions. TNF-α and IL-6 were interpreted as stress- and inflammation-related transcripts rather than as evidence of uniform NF-κB pathway inhibition. Data are mean ± SD, n = 3. *P < 0.05, **P < 0.01 vs. control; ##P < 0.01 vs. NCTD 40 μg/mL.

analyzed. Differential expression analysis identified substantial transcriptional divergence between tumor and normal tissues, with NF-κB pathway components prominently represented among the dysregulated genes (**Figure 7A**). Core NF-κB subunits RELA, NFKBIA, and NFKB1 were significantly altered, as were BAX, BCL2, JUN, and MAPK8.

GO enrichment analysis identified biological process terms related to immune response, inflammatory signaling, leukocyte activation, and apoptotic regulation among the most significantly enriched categories (**Figure 7B**). KEGG pathway analysis identified NF-κB signaling, apoptosis, TNF signaling, and MAPK signaling among the most significantly enriched pathways (**Figure 7C**).

NF-κB activity correlates with immune microenvironment features in HCC

ssGSEA-based deconvolution of 22 immune cell types revealed significant compositional shifts between tumor and normal tissues (**Figure 8A**). Resting memory CD4+ T cells, M0 macrophages, and resting dendritic cells were enriched in tumor samples, whereas activated NK cells, M1 macrophages, and activated mast cells were relatively depleted. The per-sample immune composition is shown as a stacked bar plot in **Figure 8B**.

The ssGSEA-derived NF-κB Core activity score, calculated from RELA, NFKBIA, NFKB1, IKBKB, CHUK, RELB, and NFKB2, showed overlapping distributions between tumor and normal tissues, and the difference was not statistically significant (Wilcoxon P = 0.2304819; **Figure 8C**). This result indicates that the selected bulk RNA-seq core-gene score did not show a global tumor-normal shift, and does not exclude context-specific NF-κB activation at the protein, subcellular, or microenvironmental level. Spearman correlation analysis showed positive associations between NF-κB activity and several immune cell infiltration scores, including acti-

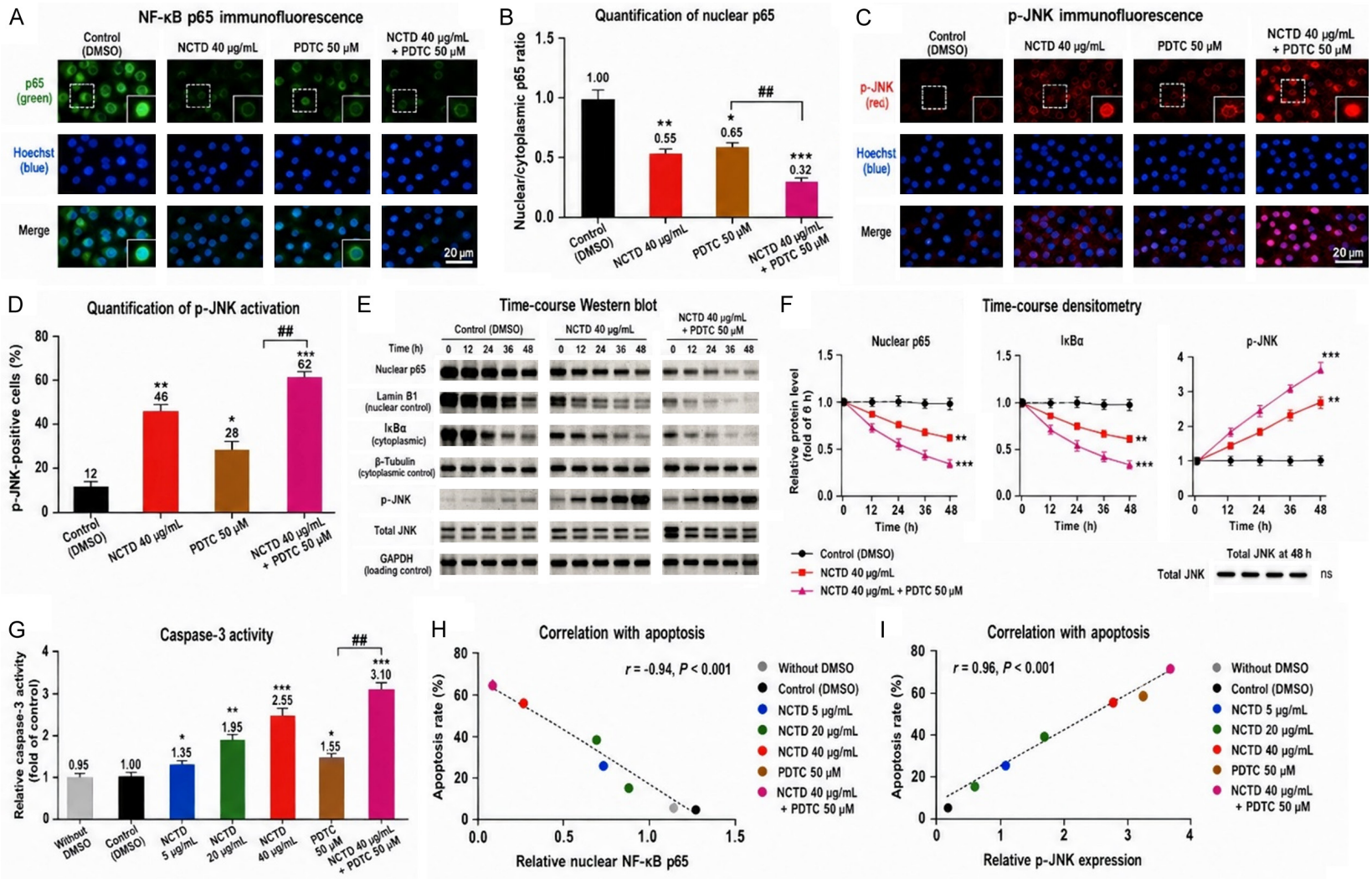

Figure 5. Reduced nuclear p65 signal is associated with enhanced NCTD-induced JNK activation and apoptosis. (A) Immunofluorescence of NF-κB p65 (green) and p-JNK (red) in MHCC97-H cells treated with NCTD (40 μg/mL), PDTC (50 μM), or their combination for 24 h; Hoechst 33342 (blue) was used as a nuclear counterstain to visualize apoptotic morphology, including chromatin condensation and nuclear fragmentation. (B, D) Quantification of nuclear p65 (B) and p-JNK-positive cells (D). (C) p-JNK immunofluorescence under the same conditions. (E, F) Time-course Western blotting (E) and densitometric analysis (F) of nuclear p65, cytoplasmic IκBα, p-JNK, and total JNK over 0-48 h. (G) Caspase-3/7 activity. (H, I) Pearson correlation between nuclear p65 (H) or p-JNK (I) levels and apoptosis rate across treatment groups. Data are mean ± SD, n = 3. *P < 0.05, **P < 0.01, ***P < 0.001 vs. control; ##P < 0.01 vs. NCTD 40 μg/mL.

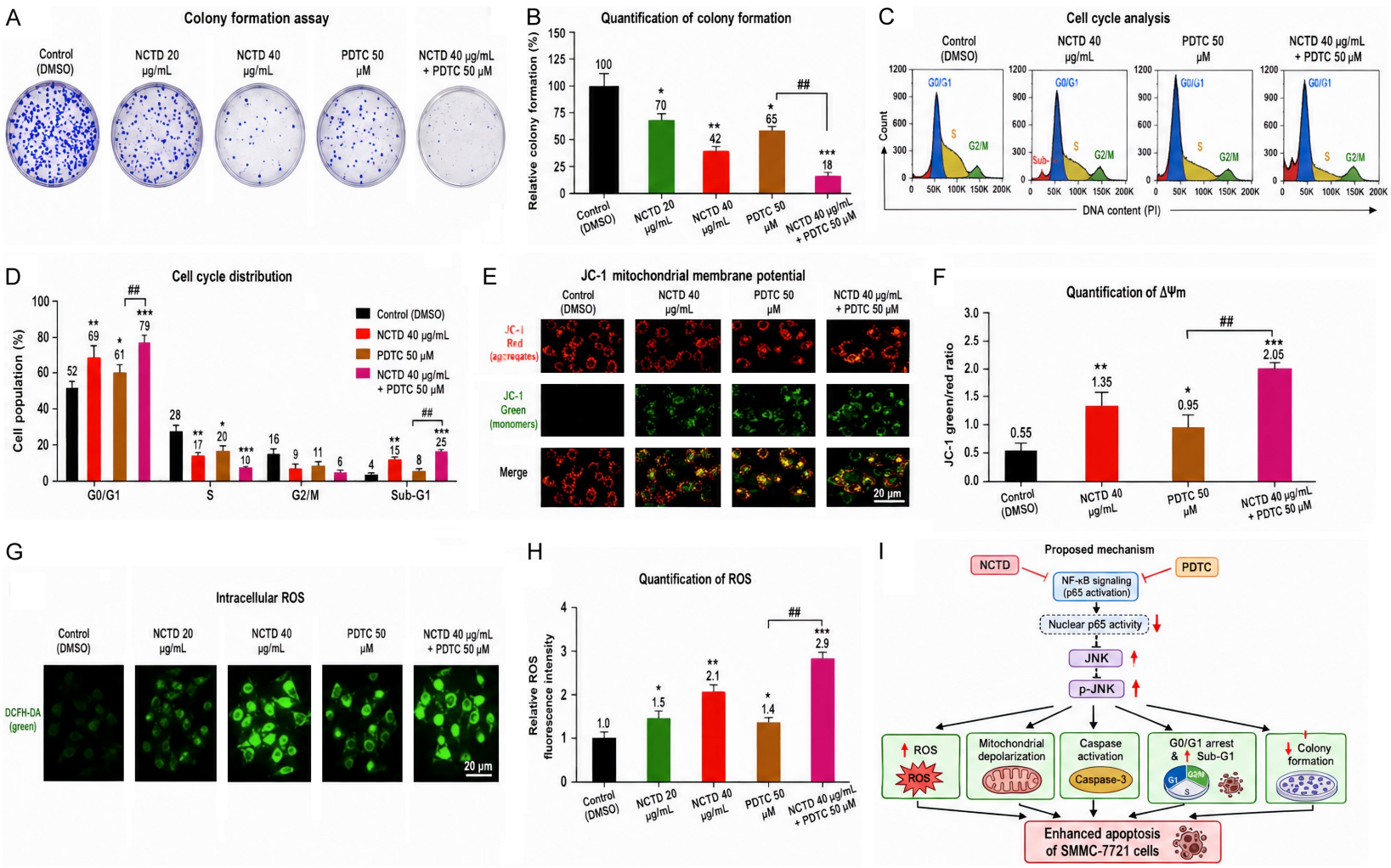

Figure 6. NCTD impairs colony formation, induces cell-cycle arrest, and triggers mitochondrial dysfunction. A, B. Colony formation assay. C, D. Cell-cycle distribution by flow cytometry. E, F. JC-1 staining for mitochondrial membrane potential. G, H. CM-H_2DCFDA detection of intracellular ROS. I. Schematic of the proposed mechanism. Data are mean ± SD, n = 3. *P < 0.05, **P < 0.01, ***P < 0.001 vs. control; ##P < 0.01, ###P < 0.001 vs. NCTD 40 μg/mL.

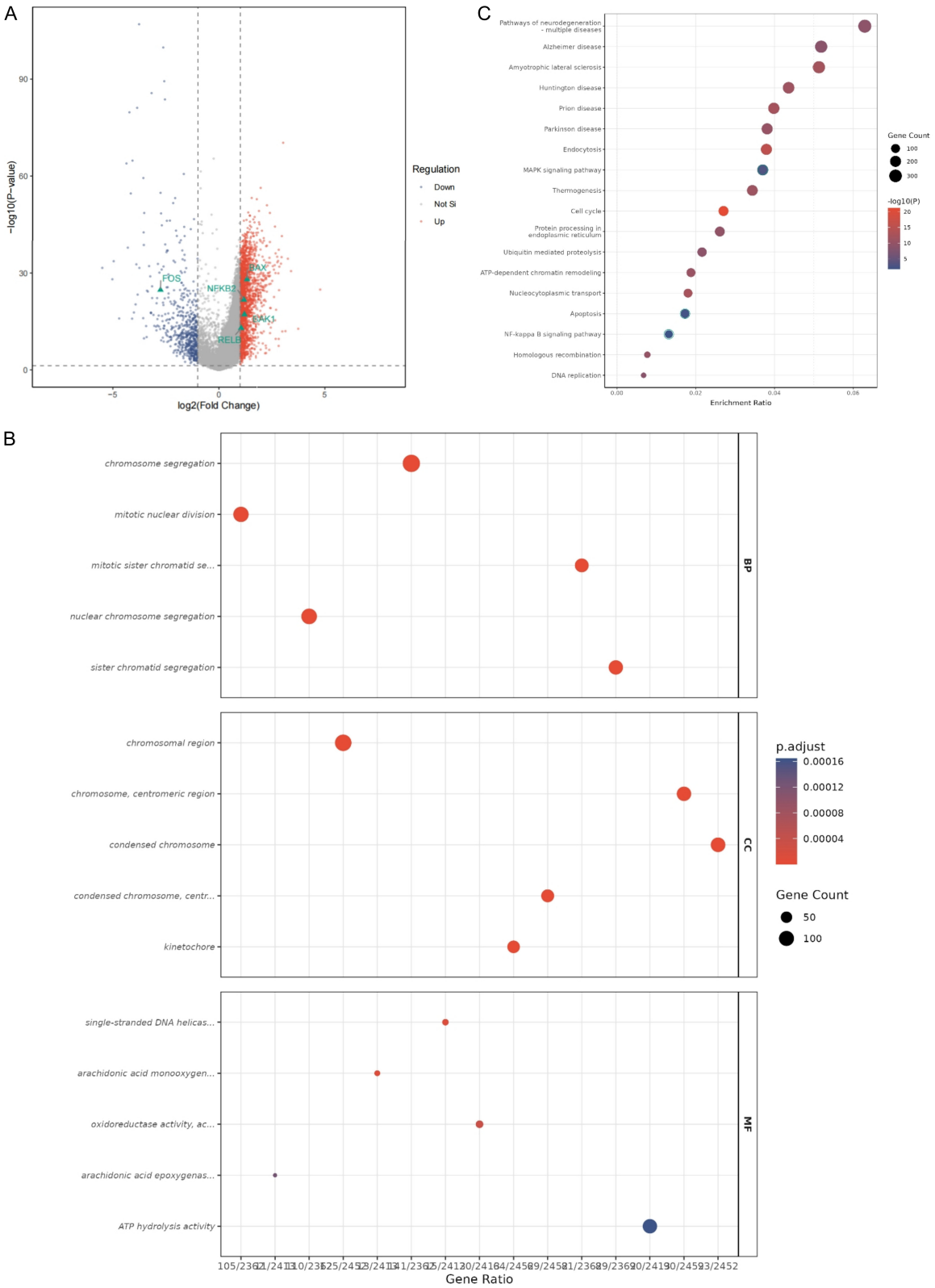

Figure 7. TCGA-LIHC analysis of NF-κB pathway dysregulation in HCC. A. Volcano plot of differentially expressed genes between 374 HCC tumors and 50 normal tissues; NF-κB pathway genes with significant differential expression are highlighted. B. GO enrichment analysis (BP, CC, and MF) of DEGs. C. KEGG pathway enrichment analysis; NF-κB, apoptosis, and TNF signaling pathways were among the enriched terms.

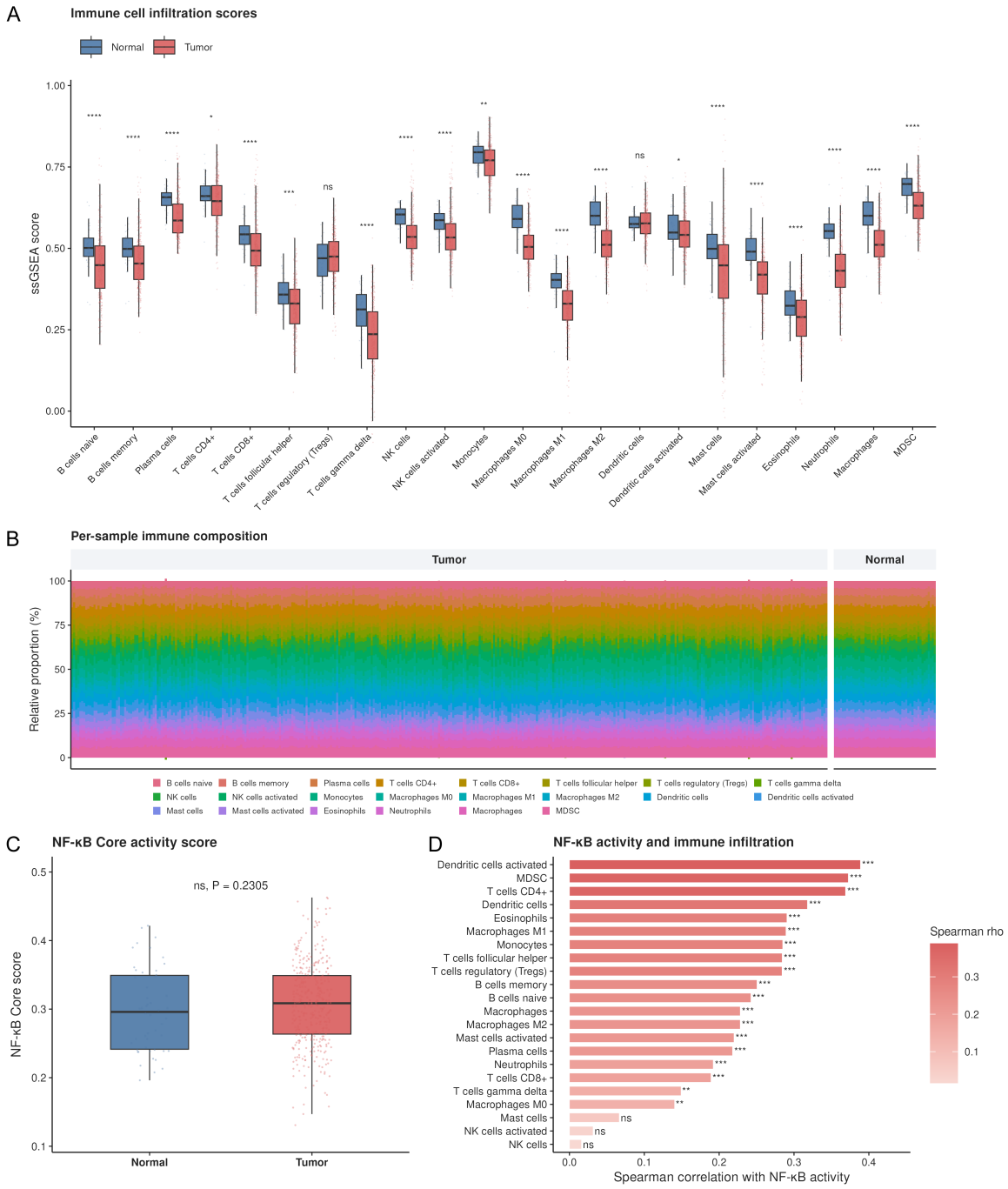

Figure 8. Immune microenvironment features and NF-κB activity correlations in HCC. A. Boxplots of ssGSEA immune cell infiltration scores for 22 immune cell types in tumor versus normal tissues. B. Stacked bar chart of immune cell composition per sample. C. Tumor-versus-normal distribution of the NF-κB Core activity score calculated from RELA, NFKBIA, NFKB1, IKBKB, CHUK, RELB, and NFKB2. D. Spearman correlation between NF-κB pathway activity scores and immune cell infiltration scores. Bar color represents the Spearman correlation coefficient. *P < 0.05, **P < 0.01, ***P < 0.001, ****P < 0.0001; ns, not significant.

vated dendritic cells, MDSCs, CD4+ T cells, dendritic cells, eosinophils, and M1 macrophages, whereas NK cell scores were not significantly correlated (**Figure 8D**).

Discussion

The molecular pathogenesis of HCC involves multiple signaling pathways that promote un-

controlled proliferation and resistance to regulated cell death. NCTD remains of interest because of its anticancer activity and reduced toxicity profile compared with cantharidin. In the present study, NCTD reduced MHCC97-H cell viability and promoted apoptosis-related phenotypes in association with reduced nuclear p65 signal and increased JNK phosphorylation.

These results support previous observations in HCC models [18] by showing that NCTD inhibits MHCC97-H cell growth and promotes apoptosis-related pathways in a dose- and time-dependent manner. Hoechst staining revealed chromatin condensation, nuclear fragmentation, and apoptotic bodies, while Annexin V/PI flow cytometry quantified apoptosis across the concentration range. The present study extends earlier work by examining the interaction between NF-κB and JNK signaling under NCTD treatment with PDTC as a pathway-directed pharmacologic tool.

NF-κB has a context-dependent role in liver biology: it supports hepatocyte survival during injury, but persistent activation in chronically damaged liver tissue can promote malignant transformation and therapeutic resistance. In the canonical activation cascade, phosphorylation and degradation of IκBα allow p65 nuclear translocation and target gene activation [19]. In our experiments, both nuclear p65 signal and cytoplasmic IκBα decreased after NCTD treatment. Therefore, the IκBα result should not be interpreted as direct evidence of simple canonical NF-κB pathway blockade. Rather, the data indicate reduced nuclear p65-associated signal together with altered IκBα turnover under drug-induced stress and apoptosis [20]. The observed increase in p-JNK, with unchanged total JNK, suggests phosphorylation-dependent JNK activation. These changes were enhanced by PDTC, suggesting that modulation of nuclear p65-associated signaling and oxidative-stress responses may be linked to, but does not by itself prove direct causation of, JNK activation.

The transcriptional data further support an apoptosis- and stress-associated response. Bax and Bcl-2 were reciprocally regulated, increasing the Bax/Bcl-2 ratio in a direction consistent with mitochondrial apoptotic priming. c-Jun induction supports functional engagement of the JNK pathway. The upregulation of TNF-α and IL-6 should not be treated as direct evidence of NF-κB inhibition; instead, it may reflect stress-associated inflammatory transcription involving JNK/AP-1 signaling and residual or context-dependent NF-κB-related activity during drug-induced apoptosis.

These functional assays extended the molecular findings to phenotypic endpoints relevant to tumor biology. Reduced colony formation indicates impaired long-term reproductive capacity rather than a transient stress response. G0/G1 accumulation and the increased sub-G1 fraction were consistent with cell-cycle blockade and apoptotic DNA loss. JC-1 and CM-H_2DCFDA staining further showed mitochondrial depolarization and ROS accumulation, supporting involvement of the mitochondrial apoptosis pathway. The stronger effects observed with PDTC co-treatment may reflect combined modulation of nuclear p65-associated signaling and oxidative-stress responses, although additional mechanistic experiments are required to define the direct pathway relationships.

The TCGA analysis provides cohort-level context for the in vitro findings. Differential expression of NF-κB pathway genes in HCC tumors and enrichment of NF-κB-, apoptosis-, TNF-, and MAPK-related pathways suggest that this signaling network is relevant to clinical HCC [21]. Associations between NF-κB activity profiles and tumor-infiltrating immune cell patterns further support a relationship between NF-κB-related transcriptional programs and the tumor microenvironment [22]. These bioinformatic findings are correlative and should be interpreted as supportive clinical-context evidence rather than experimental validation [23].

Several limitations in this work should be acknowledged. All in vitro experiments were performed in a single HCC cell line, and validation in additional HCC cell lines and normal hepatocytes will be required to assess generalizability and the therapeutic window. Because MHCC97-H is a highly metastatic HCC cell line, signaling events such as JNK activation may also influence motility-related phenotypes; migration and invasion assays were not performed in this study and should be addressed in future work. The data show concurrent reduction in nuclear p65 signal and activation of JNK phosphorylation during NCTD treatment,

but the direct molecular relationship between these events remains uncertain and will require co-immunoprecipitation, kinase inhibitor screening, or genetic loss-of-function studies. In vivo models were not included, and future studies should evaluate pharmacodynamic modulation of NF-κB/JNK signaling in tumor tissue. Finally, the TCGA analysis is correlative and should be interpreted as supportive clinical-context evidence rather than experimental validation.

In conclusion, this study indicates that NCTD induces apoptosis in MHCC97-H HCC cells in association with attenuation of nuclear p65-related NF-κB signaling and enhancement of JNK phosphorylation during mitochondrial apoptosis [6]. The TCGA-LIHC analysis provides supportive clinical-context evidence for the relevance of this signaling network and its association with the HCC immune microenvironment. These findings support further investigation of NCTD-related therapeutic strategies and the NF-κB/JNK signaling interface in HCC.

Acknowledgements

This work was supported by the Young Scientists Fund of the National Natural Science Foundation of China (Grant No. 81900522).

Disclosure of conflict of interest

None.

Address correspondence to: Donglai Cui, Department of Gastroenterology, The Second Hospital of Hebei Medical University, Shijiazhuang 050035, Hebei, China. E-mail: donglaicui1992@outlook.com

References

[1] Huang DQ, Mathurin P, Cortez-Pinto H and Loomba R. Global epidemiology of alcohol-associated cirrhosis and HCC: trends, projections and risk factors. Nat Rev Gastroenterol Hepatol 2023; 20: 37-49.

[2] Toh MR, Wong EYT, Wong SH, Ng AWT, Loo LH, Chow PK and Ngeow J. Global epidemiology and genetics of hepatocellular carcinoma. Gastroenterology 2023; 164: 766-782.

[3] Wang G, Dong J and Deng L. Overview of cantharidin and its analogues. Curr Med Chem 2018; 25: 2034-2044.

[4] Pan MS, Cao J and Fan YZ. Insight into norcantharidin, a small-molecule synthetic compound with potential multi-target anticancer activities. Chin Med 2020; 15: 55.

[5] Zhang F, Chen X, Qiao C, Yang S, Zhai Y, Zhang J, Chai K, Wang H, Zhou J, Guo M, Lu P and Wu J. Exploring the anti-colorectal cancer mechanism of norcantharidin through TRAF5/NF-κB pathway regulation and folate-targeted liposomal delivery. Int J Mol Sci 2025; 26: 1450.

[6] Qian ZM, Chen YJ and Bao YX. Pharmacological mechanisms of norcantharidin against hepatocellular carcinoma. Am J Cancer Res 2023; 13: 5024-5038.

[7] Ren J, Li G, Zhao W, Lin L and Ye T. Norcantharidin combined with ABT-737 for hepatocellular carcinoma: therapeutic effects and molecular mechanisms. World J Gastroenterol 2016; 22: 3962-3968.

[8] Arsura M and Cavin LG. Nuclear factor-kappaB and liver carcinogenesis. Cancer Lett 2005; 229: 157-169.

[9] Mathes E, O'Dea EL, Hoffmann A and Ghosh G. NF-kappaB dictates the degradation pathway of IkappaBalpha. EMBO J 2008; 27: 1357-1367.

[10] Luedde T and Schwabe RF. NF-κB in the liver--linking injury, fibrosis and hepatocellular carcinoma. Nat Rev Gastroenterol Hepatol 2011; 8: 108-118.

[11] Yue J and López JM. Understanding MAPK signaling pathways in apoptosis. Int J Mol Sci 2020; 21: 2346.

[12] Nakano H, Nakajima A, Sakon-Komazawa S, Piao JH, Xue X and Okumura K. Reactive oxygen species mediate crosstalk between NF-kappaB and JNK. Cell Death Differ 2006; 13: 730-737.

[13] Colaprico A, Silva TC, Olsen C, Garofano L, Cava C, Garolini D, Sabedot TS, Malta TM, Pagnotta SM, Castiglioni I, Ceccarelli M, Bontempi G and Noushmehr H. TCGAbiolinks: an R/Bioconductor package for integrative analysis of TCGA data. Nucleic Acids Res 2016; 44: e71.

[14] Ritchie ME, Phipson B, Wu D, Hu Y, Law CW, Shi W and Smyth GK. Limma powers differential expression analyses for RNA-sequencing and microarray studies. Nucleic Acids Res 2015; 43: e47.

[15] Yu G, Wang LG, Han Y and He QY. clusterProfiler: an R package for comparing biological themes among gene clusters. OMICS 2012; 16: 284-287.

[16] Hänzelmann S, Castelo R and Guinney J. GSVA: gene set variation analysis for microarray and RNA-seq data. BMC Bioinformatics 2013; 14: 7.

[17] Nakano H. Signaling crosstalk between NF-kappaB and JNK. Trends Immunol 2004; 25: 402-405.

[18] Yousef EH, El-Magd NFA and El Gayar AM. Norcantharidin potentiates sorafenib antitumor activity in hepatocellular carcinoma rat

model through inhibiting IL-6/STAT3 pathway. Transl Res 2023; 260: 69-82.
[19] Hayden MS and Ghosh S. Shared principles in NF-kappaB signaling. Cell 2008; 132: 344-362.
[20] Dong X, Li JC, Jiang YY, Xia MY, Tashiro S, Onodera S and Ikejima T. p38-NF-κB-promoted mitochondria-associated apoptosis and G2/M cell cycle arrest in norcantharidin-treated HeLa cells. J Asian Nat Prod Res 2012; 14: 1008-1019.
[21] Cancer Genome Atlas Research Network. Electronic address: wheeler@bcm.edu; Cancer Genome Atlas Research Network. Comprehensive and integrative genomic characterization of hepatocellular carcinoma. Cell 2017; 169: 1327-1341, e1323.
[22] Yang D, Zhou Y, Zhang Y, Su Y, Shen J, Yu B, Zhao K and Ding Y. Comprehensive analysis of scRNA-Seq and bulk RNA-Seq data reveals dynamic changes in tumor-associated neutrophils in the tumor microenvironment of hepatocellular carcinoma and leads to the establishment of a neutrophil-related prognostic model. Cancer Immunol Immunother 2023; 72: 4323-4335.
[23] Neelgundmath M, Dinesh KR, Mohan CD, Li F, Dai X, Siveen KS, Paricharak S, Mason DJ, Fuchs JE, Sethi G, Bender A, Rangappa KS, Kotresh O and Basappa. Novel synthetic coumarins that targets NF-κB in Hepatocellular carcinoma. Bioorg Med Chem Lett 2015; 25: 893-897.